Journal of Nuclear Medicine, published on September 13, 2018 as doi:10.2967/jnumed.118.210518

Amyloid Load – a more sensitive biomarker for amyloid imaging

Alex Whittington[1,2], Roger N. Gunn[1,2,3,*]; Alzheimer's Disease Neuroimaging Initiative

1. Division of Brain Sciences, Imperial College London, Hammersmith Hospital Campus, London, UK
2. Invicro Ltd, London, UK
3. Department of Engineering Science, Institute of Biomedical Engineering, University of Oxford, Oxford, UK.

Corresponding author

Alex Whittington,
Division of Brain Sciences, Burlington Danes Building,
Hammersmith Hospital, Du Cane Road,
London, W12 0NN, UK.
Email: a.whittingon13@imperial.ac.uk

Data used in preparation of this article were obtained from the Alzheimer's Disease Neuroimaging Initiative (ADNI) database (adni.loni.usc.edu). As such, the investigators within the ADNI contributed to the design and implementation of ADNI and/or provided data but did not participate in analysis or writing of this report. A complete listing of ADNI investigators can be found at: http://adni.loni.usc.edu/wp-content/uploads/how_to_apply/ADNI_Acknowledgement_List.pdf

Abstract

Amyloid-β (Aβ) plays a key role in the pathogenesis of Alzheimer's disease (AD) and it can be imaged *in vivo* using [^{18}F]Florbetapir positron emission tomography (PET). A composite standardised uptake value ratio (SUVr) is a commonly used outcome measure for quantifying the global Aβ burden however the sensitivity is sub-optimal which can lead to low power in clinical trials. We introduce amyloid load, $A\beta_L$ as a novel biomarker to quantify the global Aβ burden along with an automated algorithm for its calculation (Amyloid^{IQ}).

$A\beta_L$ is evaluated on cross-sectional and longitudinal data obtained from the Alzheimer's disease neuroimaging initiative (ADNI). The cross-sectional data consisted of 769 subjects across the disease spectrum (211 healthy controls (HC), 223 early mild cognitive impairment (EMCI), 204 late mild cognitive impairment (LMCI), 132 AD). The distributions of $A\beta_L$ in the four different classifications were compared and the same analyses were applied to a composite SUVr outcome measure. The effect sizes (hedges' g) between all but one classifications were higher for $A\beta_L$ than composite SUVr with the mean difference in effect size being 46%. 147 of the EMCI patients had a two-year follow-up scan and the effect size between baseline and follow-up for $A\beta_L$ was 0.49 compared to 0.36 for a composite SUVr demonstrating an equivalent increase in power for longitudinal data.

These results provide evidence that $A\beta_L$ will be a valuable outcome measure in future Aβ imaging studies providing an substantial increase in power over currently employed SUVr methods.

Introduction

Neuritic plaques are one of two pathological hallmarks of Alzheimer's disease (AD) and the major constituent of these plaques is amyloid-β (Aβ)(*1–3*). Evidence suggests Aβ plays a key role in the pathogenesis of the disease(*4–6*).

The *in vivo* Aβ concentration can be quantified in humans with static Positron Emission Tomography (PET) image using the radioligand [^{18}F]Florbetapir. A composite SUVr with a grey matter cerebellum reference region is a commonly used outcome measure for assessing the global Aβ burden from static images. It can be calculated from a static [^{18}F]Florbetapir image by dividing the mean intensity of voxels in a Aβ specific target region which includes the majority of the cortex by the mean intensity of voxels in the grey matter cerebellum where these two regions of interest have been defined using a combination of a grey matter probability and an anatomical atlas.

Large cross-sectional, longitudinal studies have been performed with composite SUVr as the primary outcome measure(*7–9*) in order to better understand the Aβ accumulation in AD. Whilst the cross-sectional studies have shown increases in composite SUVr in AD subjects when compared to healthy controls(*7*,*10*), the longitudinal results show high variability(*11*,*12*) between baseline and follow-up. High variability in the outcome measure results in low power to detect biological differences in the Aβ concentration. As a result of this, it has been argued that only dynamic images should be used for quantitative imaging studies(*13*) but this is less cost-effective and puts more stress on patients. A more sensitive outcome measure from static [^{18}F]Florbetapir PET images

which quantifies the global Aβ burden could reduce variability and therefore increase the probability of detecting real biological effects.

In this work, we introduce a novel sensitive biomarker, $A\beta_L$ for quantifying the global Aβ burden from static [^{18}F]Florbetapir PET images. It is calculated using two previously derived canonical images for the non-specific binding of [^{18}F]Florbetapir and the Aβ carrying capacity(*14*). $A\beta_L$ is calculated using the fully automated Amyloid^{IQ} algorithm on both cross-sectional and longitudinal data from the Alzheimer's disease neuroimaging initiative (ADNI) and the results from $A\beta_L$ are compared to those from composite SUVr.

Materials and methods

Imaging data

Cross-sectional data - [^{18}F]Florbetapir human Aβ PET imaging data and structural Magnetic Resonance Imaging (MRI) data were obtained from the (ADNI) database(*15*) (adni.loni.usc.edu) for 779 subjects (211 healthy controls (HC), 223 early mild cognitive impairment (EMCI), 204 late mild cognitive impairment (LMCI), 132 AD)

Longitudinal data – In addition to the cross-sectional data, two year follow-up (mean 1.96 ±(0.12) years) scans for 147 subjects were downloaded.

The ADNI was launched in 2003 as a public-private partnership, led by Principal Investigator Michael W. Weiner, MD. The primary goal of ADNI has been to test whether serial MRI, PET, other biological markers, and clinical and neuropsychological assessment can be combined to measure the progression of mild cognitive impairment and early AD. For up-to-date information, see www.adni-info.org.

[^{18}F]Florbetapir human $A\beta$ PET imaging data - [^{18}F]Florbetapir PET scans consisted of a 20-minute [^{18}F]Florbetapir PET scan 50 minutes post-injection (370±37 MBq) according to the standardised ADNI protocol(*7*). There were 3 image pre-processing steps applied to the data prior to entry into the ADNI imaging database (For full details, see http://adni.loni.usc.edu/methods/pet-analysis/pre-processing). Briefly, 4 late-time 5 minute frames are co-registered and averaged. The resulting image is converted to a 160x160x96 voxel static image with voxel dimension of 1.5mmx1.5mmx1.5mm.

Finally, an 8mm full width half maximum gaussian filter was applied (corresponding to the lowest resolution scanner used in the study). These primary data were downloaded from the ADNI database and used in the subsequent analyses.

T1-weighted Magnetic Resonance Imaging data – All subjects underwent T1-weighted 1.5T structural MRI which were downloaded from the ADNI imaging database.

Image Processing

Registration of images into streotactic space - [^{18}F]Florbetapir data were nonlinearly registered into Montreal Neurological Institute 152 space (MNI152 space(*16*)) using a diffeomorphic nonlinear registration (DARTEL)(*17*). Initially, the structural MRI images were segmented into grey matter and white matter using SPM12 and registered to a group average template. The group average template was then registered to MNI152 space. Each [^{18}F]Florbetapir SUVr image was registered to the their corresponding MRI using a rigid-body registration. Finally, the individuals' DARTEL flow field and template transformation was applied without modulation resulting in [^{18}F]Florbetapir images in MNI152 space. The normalised maps were spatially smoothed (8mm full width at half maximum (FWHM) Gaussian kernel). Each registration was visually assessed to check the quality of the registration. 10 subjects were rejected which meant the cross-sectional dataset used included 769 subjects and the longitudinal dataset included 147 subjects.

Generation of SUVr images - SUVr images for all scans were generated using the grey matter cerebellum as the reference region which was defined as the intersection between

the cerebellum ROI of the CIC atlas(*18*) and the grey matter atlas with p(grey matter) > 0.3. The mean uptake value for the grey matter cerebellum ROI was obtained and image intensities were divided by this to generate an SUVr image for each subject.

Definition of $A\beta_L$

Based on our prior spatiotemporal modeling work(*14*) we hypothesized that a [^{18}F]Florbetapir SUVr (grey matter cerebellum reference) image, spatially normalised into MNI152 space, could be effectively modelled using a linear combination of previously derived canonical images for the non-specific binding **NS** and carrying capacity **K**(*19*). Therefore,

$$\mathbf{SUVr_{fit}} = ns\mathbf{NS} + A\beta_L\mathbf{K} \quad (1)$$

where, $\mathbf{SUVr_{fit}}$ is the modelled image, **NS** is the non-specific binding image, **K** is the carrying capacity image, ns is the non-specific binding coefficient and $A\beta_L$ is the amyloid load. As the carrying capacity image is the one relating to Aβ concentration, it was further hypothesised, that the $A\beta_L$ would be a sensitive biomarker to quantify the global Aβ burden ranging from 0% in the case of a healthy brain up to 100% in the case of a brain with the highest level of amyloid.

Amyloid^{IQ} algorithm for calculating $A\beta_L$

After spatially normalising the [^{18}F]Florbetapir SUVr images, a fully automated algorithm was used to calculate $\mathbf{SUVr_{fit}}$, ns and $A\beta_L$ for each image. Values for ns and

$A\beta_L$ were optimised by minimising the sum of squares of residuals between the voxel intensities of the spatially normalised [^{18}F]Florbetapir SUVr image and the $\mathbf{SUVr_{fit}}$ image. This was achieved by forming the overdetermined system of linear equations shown in equation 2 and solving for ns and $A\beta_L$. Equation 2 was optimised in MATLAB using QR decomposition.

$$\begin{bmatrix} NS_1 & K_1 \\ \vdots & \vdots \\ NS_{end} & K_{end} \end{bmatrix} \begin{bmatrix} ns \\ \mathrm{A\beta_L} \end{bmatrix} = \begin{bmatrix} SUVr_1 \\ \vdots \\ SUVr_{end} \end{bmatrix} \quad (2)$$

where NS_i, K_i and $SUVr_i$ are the i^{th} voxel intensities in the **NS** image, **K** image and [^{18}F]Florbetapir SUVr image in MNI space respectively.

The algorithm produces four outputs as summarised in Figure 1. The parameter values ns and $\mathrm{A\beta_L}$ are estimated along with the fitted image ($\mathbf{SUVr_{fit}}$) and the residual difference ($\mathbf{SUVr - SUVr_{fit}}$).

Comparison of $A\beta_L$ with composite SUVr

In both the cross-sectional and longitudinal studies, $A\beta_L$ was compared to composite SUVr as an outcome measure to quantify the Aβ burden.

A composite SUVr was defined to be the mean SUVr value from grey matter voxels (those with p(grey matter)>0.3) in 4 large cortical regions (Frontal lobe excluding

Sensory Motor Area and Precentral gyrus, Cingulate cortex, Parietal Lobe and Temporal Lobe) taken from the CIC atlas(*18*).

In the cross-sectional study, the effect sizes (hedges g) were calculated between each of the different clinical groups for both $A\beta_L$ and composite SUVr. For the longitudinal study, an effect size (again hedges g) was calculated for the delta of follow-up from baseline for both $A\beta_L$ and composite SUVr.

Results

Calculation of $A\beta_L$

$A\beta_L$ was successfully calculated for all 769 subjects, the algorithm was completed for each subject in under 1 minute on a standard workstation after the PET images had been spatially normalised to MNI space (where the canonical images **K** and **NS** had been generated previously).

Evaluation of $\mathbf{SUVr_{fit}}$ images

The quality of the fit for $\mathbf{SUVr_{fit}}$ was assessed by evaluating the percentage voxels in the brain which satisfied $|\mathbf{SUVr} - \mathbf{SUVr_{fit}}| > 0.3$ (see Figure 2). The larger this percentage, the poorer the fit. The mean percentage of voxels in the brain with $|\mathbf{SUVr} - \mathbf{SUVr_{fit}}| > 0.3$ across all 769 subjects was 4.6%. 96% of the 769 subjects had fewer than 20% of voxels which satisfied $|\mathbf{SUVr} - \mathbf{SUVr_{fit}}| > 0.3$ meaning that over 80% of voxels in 96% of subjects were well modelled. The highest percentage in all the subjects was 38.0%. There was no correlation between the calculated $A\beta_L$ and the percentage of voxels which satisfied $|\mathbf{SUVr} - \mathbf{SUVr_{fit}}| > 0.3$. Example fittings for images with high, medium and low $A\beta_L$ scores can be seen in supplementary materials (Figure S1).

$\mathbf{A\beta_L}$ and composite SUVr in cross-sectional ADNI data

The distributions of $A\beta_L$ in the four different ADNI classifications (HC, EMCI, LMCI, AD) were calculated and compared to analogous distributions for the composite SUVr. Boxplots for each of the distributions are presented in Figure 3, the effect sizes between the different groups for effect sizes for composite SUVr and $A\beta_L$ are shown in Table 1

and Table 2 respectively. Both composite SUVr and $A\beta_L$ increase as the level of cognition declines in the ADNI population but $A\beta_L$ has greater sensitivity between all classification groups apart from EMCI to HC where the two measures were equivalent. The mean increase in effect size when comparing $A\beta_L$ with composite SUVr was 46% and the greatest increase was observed between LMCI and EMCI which increased by 106%.

The mean calculated ns for HC was 1.06. There was a 17% reduction in the mean calculated ns for AD when compared to HC and a 10% reduction between LMCI and HC but no difference between EMCI and HC. Boxplots for the distributions of ns can be seen in Figure 4.

$A\beta_L$ and composite SUVr in longitudinal ADNI data

$\Delta A\beta_L$ (baseline $A\beta_L$ subtracted from follow-up $A\beta_L$) and Δcomposite SUVr (baseline composite SUVr subtracted from follow-up composite SUVr) was calculated for each of the 147 subjects which had repeated [^{18}F]Florbetapir. The distributions of $\Delta A\beta_L$ and Δcomposite SUVr are shown in Figure 5. The increase in follow-up mean composite SUVr was 0.030 compared to baseline with a standard deviation of 0.12 which translates to an effect size of 0.36. The increase in follow-up $A\beta_L$ compared to baseline was 2.0% and the standard deviation was 5.8% which translates to an effect size for $\Delta A\beta_L$ of 0.49. This increase in effect size shows an increased sensitivity. There was no difference in the calculated ns between baseline and follow-up ($p > 0.8$).

Discussion

We have introduced the novel sensitive biomarker $A\beta_L$ to quantify the Aβ burden in the human brain using data from a static PET [^{18}F]Florbetapir scan. $A\beta_L$ is calculated by modelling an SUVr image as a linear combination of two canonical images - **K** and **NS**. Subsequently, $A\beta_L$ can be extracted simply as the scaling factor of the carrying capacity canonical image **K**. In addition to defining the biomarker, we have presented an automated algorithm, Amyloid^{IQ}, for calculating $A\beta_L$ which is fast and robust to execute.

In this work, we calculated $A\beta_L$ and composite SUVr for 769 scans subjects ranging across the full spectrum of disease. The effect sizes between the different disease classifications were calculated for both outcome measures with larger effect sizes observed for $A\beta_L$ in every comparison apart from EMCI to HC where the two measures were equivalent. The mean increase in effect size between the different classifications in the cross-sectional ADNI data was 46%. This increase in sensitivity would be important in future studies as one would require fewer subjects to detect a significant difference between disease groups and healthy controls. A similar increase in power was also observed for the longitudinal ADNI data. As with the cross-sectional results, the increased power could be important for future longitudinal studies and clinical trials. In particular, interventional studies one would have greater power to detect reductions in baseline Aβ. Figure 6 illustrates this by showing power curves (calculated using the effect sizes in the longitudinal data) for $A\beta_L$ and composite SUVr in a simulated clinical trial of an anti-Aβ therapeutic (50 placebo, 50 drug). The power for $A\beta_L$ reaches 80% at ~10% reduction in baseline Aβ whereas one would require ~20% reduction in Aβ to

achieve the same when using composite SUVr as the outcome measure. This will have a dramatic effect on the financial cost and disruption to patients in interventional studies and clinical trials. This comes at an important time as it has recently been reported that aducanumab reduces Aβ in AD(*20*).

The difference image produced by the algorithm allows one to analyse how well the SUVr image data was modelled. This feature can provide useful information as to whether a particular scan has an abnormal $A\beta_L$ due to poor fitting (resulting from poor registration to MNI space or lesions) for instance rather than abnormal concentrations of Aβ. This information is lacking when using composite SUVr. In this work, a voxel was considered to be poorly estimated if the absolute difference in intensity was greater than 0.3. 96% of the SUVr fitted images had fewer than 20% of voxels which were poorly fitted suggesting the SUVr fitted images accurately model the majority SUVr images.

The calculated ns in the cross-sectional analysis reduced as the subjects progressed along the AD pathway. It is possible that this is caused by reductions in white matter volume as [^{18}F]Florbetapir binds non-specifically to white matter and this has been shown to decline in AD by up to 5% per year. Further investigation would be required in order to characterise the relationship between the calculated ns and white matter atrophy.

There are some limitations that should be considered when using this technique in future studies. In particular, for interventional studies, one should consider that if the intervention affects the Aβ concentration in a spatially dependent manner (i.e., does not

reduce Aβ uniformly across the brain) then scans may not be modelled effectively using a linear combination of **NS** and **K** after treatment. The quality of fitting pre and post treatment should be investigated in future work. Also, caution should be exercised when using $A\beta_L$ disease groups other than AD as the outcome measure was developed using templates derived from modelling the disease progression of AD. In addition, it should also be noted that all the work here used SUVr images with a grey matter cerebellum reference region. Recent work has showed greater effect sizes for composite SUVr when using a white matter composite reference region (*21*) and therefore the increase in effect size of $A\beta_L$ over this SUVr measure could be reduced. However, as mentioned previously, there is a reduction in the calculated ns as the disease progresses and the use of white matter as a reference region is not without complexities that will require further investigation.

Conclusion

In conclusion, we have introduced the novel biomarker $A\beta_L$ for quantifying the global Aβ burden using static [^{18}F]Florbetapir PET data. $A\beta_L$ was tested using both cross-sectional and longitudinal data. In both sets of data, $A\beta_L$ showed increased sensitivity to differences in Aβ concentration. $A\beta_L$ could prove useful by increasing the power to detect changes in longitudinal studies and trials of novel therapeutics targeting Aβ.

Author Contributions

A.W. conducted the experiments, analysed the data and wrote the manuscript. R.N.G. designed the study, aided in data analysis and wrote the manuscript.

Acknowledgements

We would like to thank Clifford Jack for kindly providing us with the longitudinal composite SUVr data, David J. Sharp, Ilan Rabiner and Paul Matthews for helpful comments on the manuscript, Yasser Ituria and Alan Evans for interesting discussions on this topic.

Data collection and sharing for this project was funded by the Alzheimer's Disease Neuroimaging Initiative (ADNI) (National Institutes of Health Grant U01 AG024904) and DOD ADNI (Department of Defense award number W81XWH-12-2-0012). ADNI is funded by the National Institute on Aging, the National Institute of Biomedical Imaging and Bioengineering, and through generous contributions from the following: AbbVie, Alzheimer's Association; Alzheimer's Drug Discovery Foundation; Araclon Biotech; BioClinica, Inc.; Biogen; Bristol-Myers Squibb Company; CereSpir, Inc.; Cogstate; Eisai Inc.; Elan Pharmaceuticals, Inc.; Eli Lilly and Company; EuroImmun; F. Hoffmann-La Roche Ltd and its affiliated company Genentech, Inc.; Fujirebio; GE Healthcare; IXICO

Ltd.; Janssen Alzheimer Immunotherapy Research & Development, LLC.; Johnson & Johnson Pharmaceutical Research & Development LLC.; Lumosity; Lundbeck; Merck & Co., Inc.; Meso Scale Diagnostics, LLC.; NeuroRx Research; Neurotrack Technologies; Novartis Pharmaceuticals Corporation; Pfizer Inc.; Piramal Imaging; Servier; Takeda Pharmaceutical Company; and Transition Therapeutics. The Canadian Institutes of Health Research is providing funds to support ADNI clinical sites in Canada. Private sector contributions are facilitated by the Foundation for the National Institutes of Health (www.fnih.org). The grantee organization is the Northern California Institute for Research and Education, and the study is coordinated by the Alzheimer's Therapeutic Research Institute at the University of Southern California. ADNI data are disseminated by the Laboratory for Neuro Imaging at the University of Southern California.

Disclosures

Roger Gunn is a consultant for Abbvie, Biogen and Cerveau.

References

1. Glenner GG, Wong CW. Alzheimer's disease: Initial report of the purification and characterization of a novel cerebrovascular amyloid protein. *Biochem Biophys Res Commun*. 1984;120:885-890.
2. Wong DF, Rosenberg PB, Zhou Y, et al. In vivo imaging of amyloid deposition in Alzheimer disease using the radioligand 18F-AV-45 (florbetapir [corrected] F 18). *J Nucl Med*. 2010;51:913-920.
3. Wong CW, Quaranta V, Glenner GG. Neuritic plaques and cerebrovascular amyloid in Alzheimer disease are antigenically related. *Proc Natl Acad Sci U S A*. 1985;82:8729-8732.
4. Hardy JA, Higgins GA. Alzheimer's disease: the amyloid cascade hypothesis. *Sci* . 1992;256:184-185.
5. Hardy J, Allsop D. Amyloid deposition as the central event in the aetiology of Alzheimer's disease. *Trends Pharmacol Sci*. 1991;12:383-388.
6. Stefani M, Dobson CM. Protein aggregation and aggregate toxicity: new insights into protein folding, misfolding diseases and biological evolution. *J Mol Med*. 2003;81:678-699.
7. Jagust WJ, Landau SM, Koeppe RA, et al. The Alzheimer's Disease Neuroimaging Initiative 2 PET Core: 2015. *Alzheimer's Dement J Alzheimer's Assoc*. 2016;11:757-771.
8. Rowe CC, Ellis KA, Rimajova M, et al. Amyloid imaging results from the Australian Imaging, Biomarkers and Lifestyle (AIBL) study of aging. *Neurobiol Aging*. 2010;31:1275-1283.
9. Jack CR, Wiste HJ, Lesnick TG, et al. Brain β-amyloid load approaches a plateau. *Neurology*. 2013;80:890-896.
10. Mueller SG, Weiner MW, Thal LJ, et al. The Alzheimer's disease neuroimaging initiative. *Neuroimaging Clin N Am*. 2005;15:869-877.
11. Tryputsen V, DiBernardo A, Samtani M, Novak GP, Narayan VA, Raghavan N. Optimizing Regions-of-Interest Composites for Capturing Treatment Effects on Brain Amyloid in Clinical Trials. *J Alzheimers Dis*. 2015;43:809-821.
12. Landau SM, Fero A, Baker SL, et al. Measurement of Longitudinal β-Amyloid Change with 18F-Florbetapir PET and Standardized Uptake Value Ratios. *J Nucl Med*. 2015;56:567-574.
13. Lammertsma AA. Forward to the Past: The Case for Quantitative PET Imaging. *J Nucl Med*. 2017;58:1019-1024.
14. Whittington A, Sharp DJ, Gunn RN. Spatiotemporal distribution of β-amyloid in Alzheimer's disease results from heterogeneous regional carrying capacities. *J Nucl Med*. November 2017.

15. Jagust WJ, Bandy D, Chen K, et al. The Alzheimer's Disease Neuroimaging Initiative positron emission tomography core. *Alzheimer's Dement*. 2010;6:221-229.

16. Mazziotta J, Toga A, Evans A, et al. A probabilistic atlas and reference system for the human brain: International Consortium for Brain Mapping (ICBM). *Philos Trans R Soc London Ser B*. 2001;356:1293-1322.

17. Ashburner J. A fast diffeomorphic image registration algorithm. *Neuroimage*. 2007;38:95-113.

18. Tziortzi AC, Searle GE, Tzimopoulou S, et al. Imaging dopamine receptors in humans with [11C]-(+)-PHNO: Dissection of D3 signal and anatomy. *Neuroimage*. 2011;54:264-277.

19. Whittington A, Sharp DJ, Gunn RN. Spatiotemporal Distribution of β-Amyloid in Alzheimer Disease Is the Result of Heterogeneous Regional Carrying Capacities. *J Nucl Med* . 2018;59:822-827.

20. Sevigny J, Chiao P, Bussière T, et al. The antibody aducanumab reduces Aβ plaques in Alzheimer's disease. *Nature*. 2016;537:50-56.

21. Fleisher AS, Joshi AD, Sundell KL, et al. Use of white matter reference regions for detection of change in florbetapir positron emission tomography from completed phase 3 solanezumab trials. *Alzheimer's Dement J Alzheimer's Assoc*. 2017;13:1117-1124.

Figures

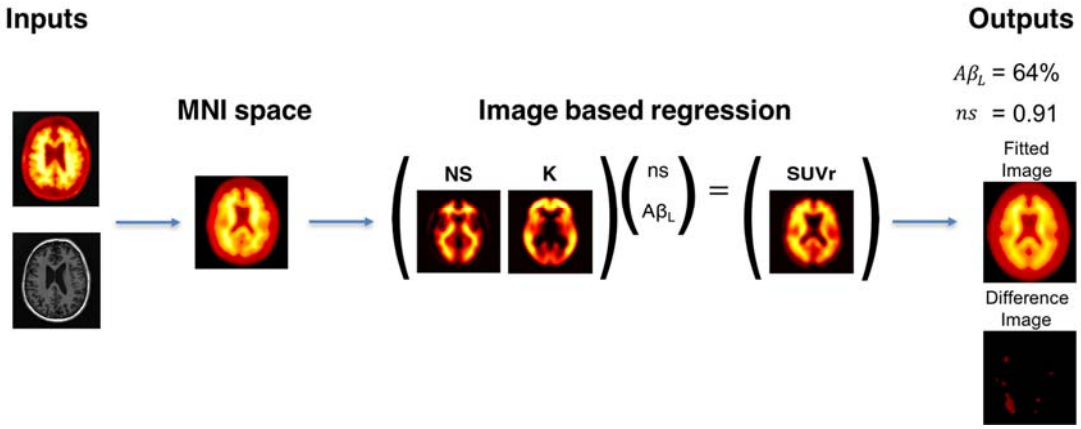

Figure 1: *Amyloid^{IQ} Algorithm for calculating $A\beta_L$ from a single SUVr image with cerebellar grey matter used a reference region.*

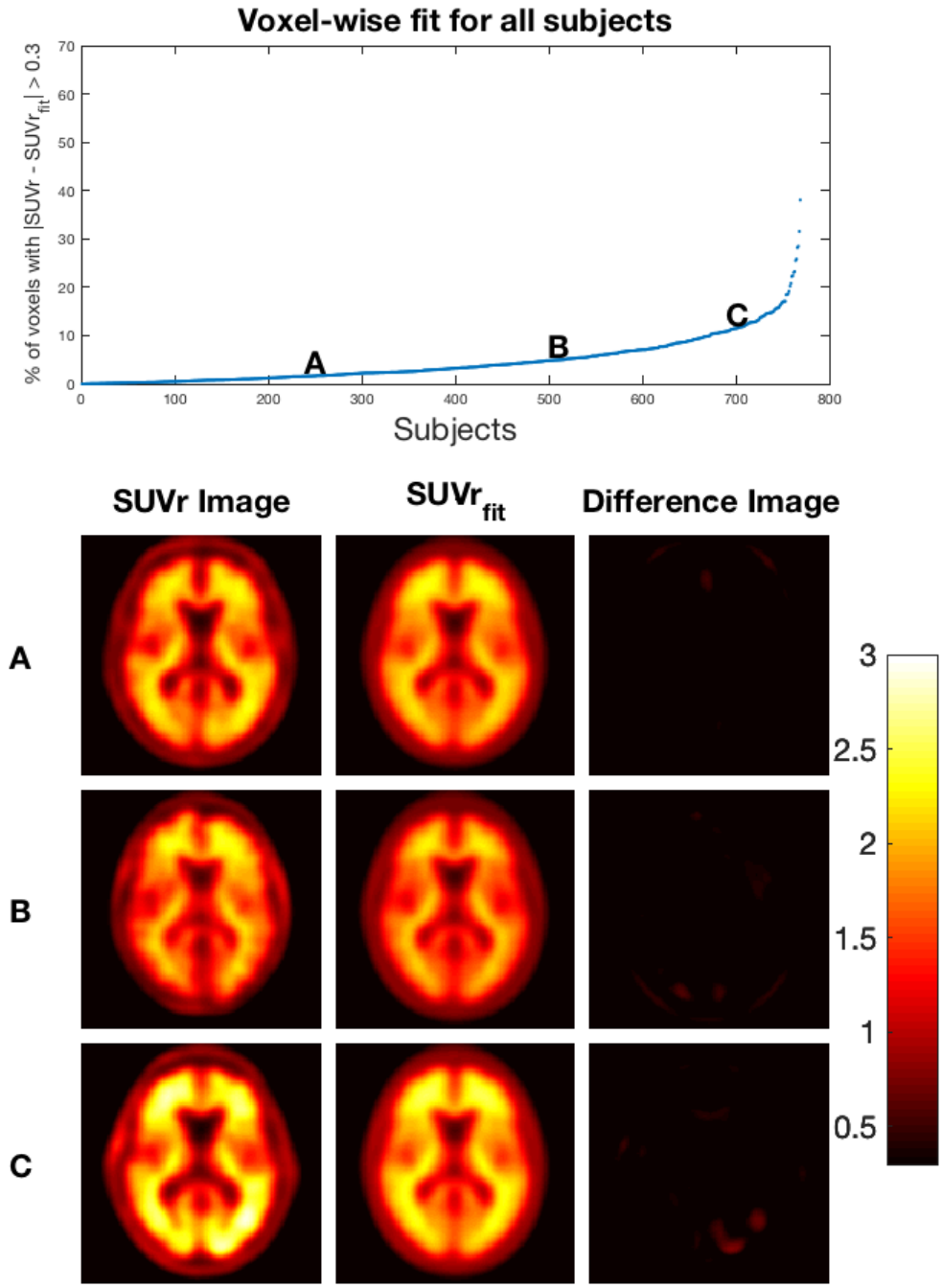

Figure 2: *Evaluation of the fit of $SUVr_{fit}$ images.* ***Top:*** *Percentage of voxels in the brain with $|SUVr - SUVr_{fit}| > 0.3$ for each subject.* ***Bottom:*** *SUVr image, the $SUVr_{fit}$ image and the difference image for three example subjects. The $SUVr_{fit}$ image accurately fits the SUVr image in all three examples.*

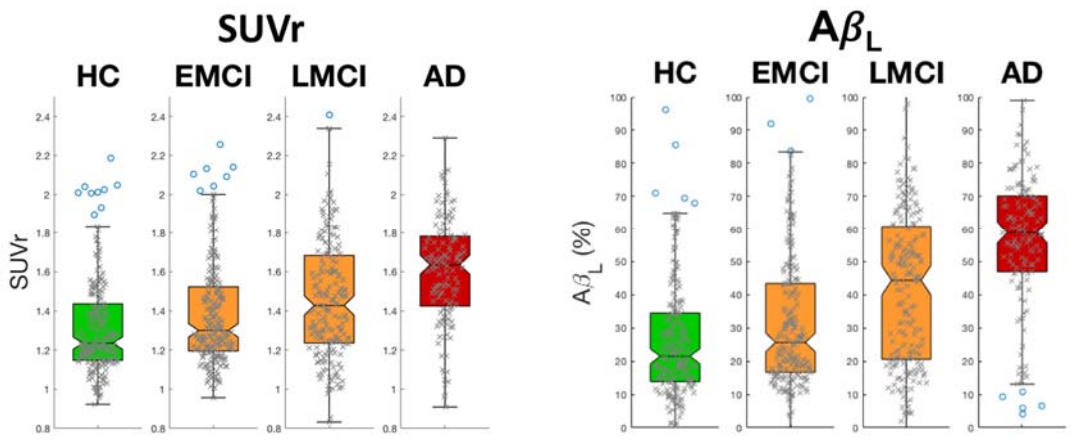

Figure 3: *Boxplots for composite SUVr (left) and $A\beta_L$ (right) for each of the four diagnosis groups in the cross-sectional data. Effect sizes are calculated between all groups are larger for $A\beta_L$ than for composite SUVr apart from EMCI to HC where the outcome measures are equivalent (see Table 1 and Table 2).*

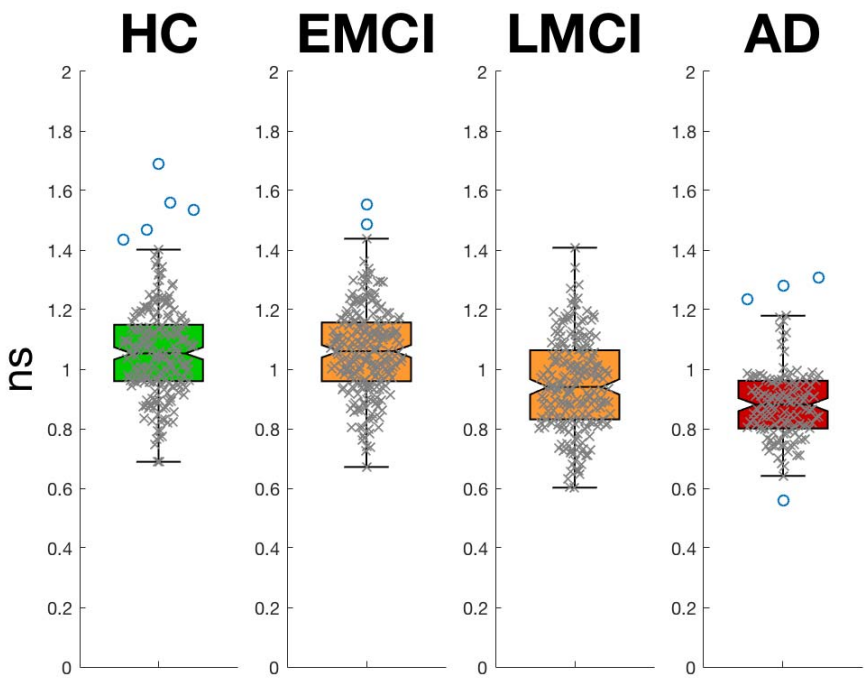

Figure 4: *Boxplots showing the distributions of ns for each of the four diagnosis groups in the cross-sectional data. ns is statistically lower in the AD and LMCI groups when compared to healthy controls but the same in the EMCI group.*

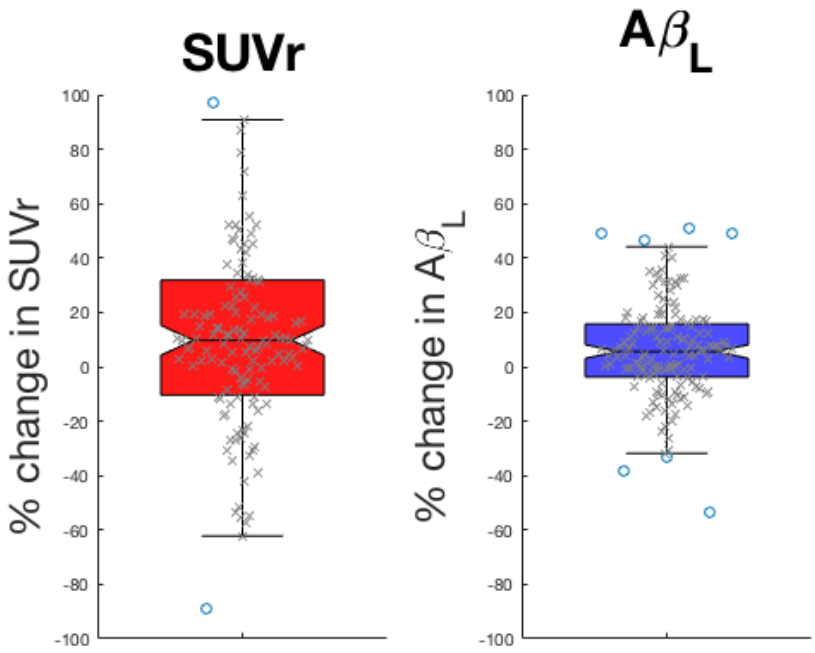

Figure 5: *Boxplots showing the distributions of % change in composite SUVr (left) and % change in $A\beta_L$ (right). A bigger effect size is demonstrated with $A\beta_L$.*

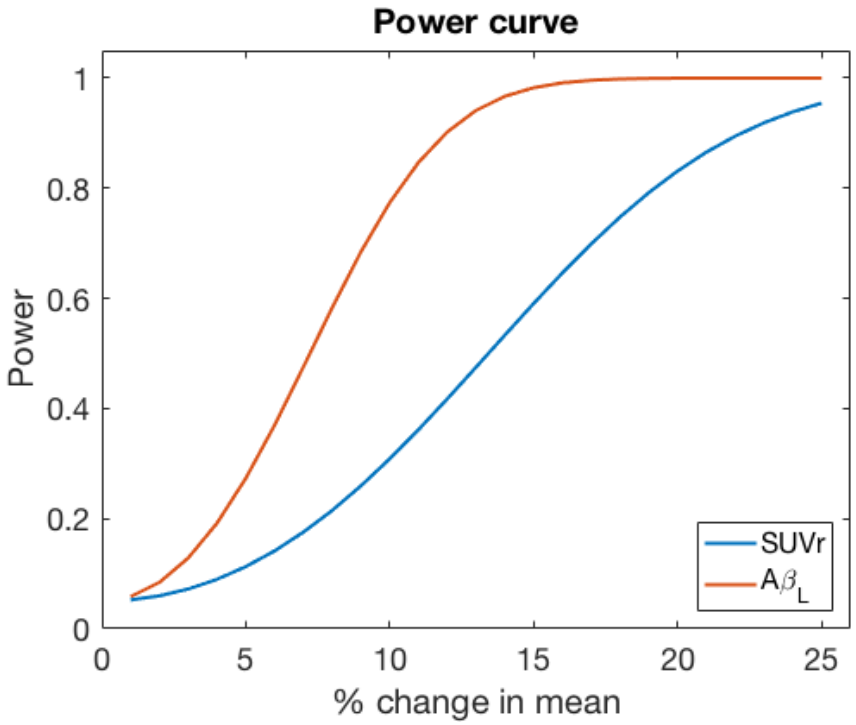

Figure 6: *Power curves for composite SUVr and $A\beta_L$ in a simulated clinical trial (50 placebo, 50 drug) of an anti-Aβ therapeutic calculated using the effect sizes found in the longitudinal ADNI data.*

Tables

	EMCI	LMCI	AD
Effect size vs HC	0.24	0.48	1.06
Effect size vs EMCI		0.26	0.81
Effect size vs LMCI			0.50

Table 1: *Table of effect sizes for composite SUVr*

	EMCI	LMCI	AD
Effect size vs HC	0.24	0.71	1.51
Effect size vs EMCI		0.49	1.24
Effect size vs LMCI			0.64

Table 2: *Table of effect sizes for* $A\beta_L$